International Journal of Materials Science

E-ISSN: 2707-823X
P-ISSN: 2707-8221
Journal's Website
IJMS 2025; 6(1): 47-52
Received: 10-01-2025
Accepted: 15-02-2025

Chandan Sahu
SSSVS Government Post Graduate College, Chunar, Mirzapur, Utter Pradesh, India

Upendra Singh
Pt. Deen Dayal Upadhyay Government Degree College, Palahipatti, Varanasi, Utter Pradesh, India

Manoj Kumar Prajapati
SSSVS Government Post Graduate College, Chunar, Mirzapur, Utter Pradesh, India

Corresponding Author:
Manoj Kumar Prajapati
SSSVS Government Post Graduate College, Chunar, Mirzapur, Utter Pradesh, India

Photoluminescence properties of $Sr_2SiO_4:Eu^{2+}$, Dy^{3+} phosphors

Chandan Sahu, Upendra Singh and Manoj Kumar Prajapati

DOI: https://www.doi.org/10.22271/27078221.2025.v6.i1a.63

Abstract
In the present paper, PL study of Dy3+ doped Sr_2SiO_4:Eu2+ phosphor is reported. A polycrystalline sample of Sr_2SiO_4:Eu2+, Dy3+ was prepared by combustion method. The obtained phosphor was characterized by powder X-ray diffraction, Scanning Electron Microscopy, UV Vis-spectroscopy, and photoluminescence. The results of the XRD studies obtained for Sr_2SiO_4:Eu2+, Dy3+ phosphor revealed its monoclinic structure. The average crystallite size was calculated as 12.77 nm. Photoluminescence study was carried out for the phosphor using UV irradiation and a single glow peak was found. The photoluminescence glow curves of the samples were measured at various concentrations of co-dopant. In this paper, the photoluminescence and afterglow behavior of these phosphors are reported.

Keywords: Photoluminescence, XRD, Spectroscopy, UV Spectroscopy, SEM

1. Introduction
Materials that present long lasting phosphorescence (LLP) are potential candidates for the use in photonics applications, such as display technology and lighting [1], especially, since the discovery of $Sr_2SiO_4:Eu^{2+}$, Dy^{3+} in the middle of the 1990s [2]. Strontium orthosilicate exits in two crystallographic structures, *viz*. α'-Sr_2SiO_4 (orthorhombic) and β-Sr_2SiO_4 (monoclinic) [3].The transition between the β-phase and the high temperature α' phase occurring at 385 K involves the rearrangement of SiO_4 tetrahedral without disconnection of the bonds [4, 5]. There are different types of scientific techniques for sample preparation, such as sol-gel [6, 7] co-precipitation and hydrothermal synthesis methods [8] which have been adjusted to phosphors. All of these methods use liquid components that can be accurately controlled and thoroughly mixed. Combustion synthesis is a fast convenient reaction with increased efficiency. In this work, combustion synthesis was used to prepare $Sr_2SiO_4:Eu^{2+}$, Dy^{3+} phosphor using urea as a fuel and NH_4Cl as a flux. The properties of $Sr_2SiO_4:Eu^{2+}$, Dy^{3+} powders were characterized by powder X-ray diffraction (XRD), scanning. lectron microscopy (SEM), and UV-Vis spectroscopy. The studies of optical properties were also performed on the basis of photoluminescence (PL).

2. Experimental
$Sr_2SiO_4:Eu^{2+}$, Dy^{3+} phosphors were synthesized by combustion method. The raw materials: strontium nitrate $Sr(NO_3)_2$, 99.99 %, silica gel 99.99 %, europium oxide Eu_2O_3, 99.99 % and dysprosium oxide Dy_2O_3, 99.99 % were used as the staring materials. The starting materials were weighted according to the stoichiometry. In addition, Eu_2O_3 and Dy_2O_3, taken as co-activators, were dissolved in concentrated nitric acid (HNO_3) before transferring them to the crucible. A small amount of ammonium chloride (NH_4Cl) was used as a flux, while the urea ($CO(NH_2)_2$) as a combustion fuel [9, 10]. The weighed quantities of each nitrate, flux and fuel were mixed in a mortar for 15 min to convert the constituents into a thick paste. The prepared paste was then placed in a vertical cylindrical muffle furnace maintained at 700 °C. Then, the prepared samples were annealed at 800 °C for 2 h under an air atmosphere. The crystalline structure size and phase composition of the samples were examined by PAN analytical diffract meter using CuKα radiation (λ = 1.5406 Å), where X-ray was generated at 40 kV/30 mA voltage and current values, respectively. The scanning electron microscopy (ZEISS EVO 18) was used to observe particle morphology of the phosphors. Absorption spectra were recorded using (Shimadzu UV-1700 UV-Vis) spectrophotometer. The samples were irradiated with UV-ray source. In photoluminescence spectra (PL), excitation and

Emission were recorded by spectrofluorometer (PerkinElmer LS45). All experiments were performed in identical conditions and it was observed that the results were reproducible.

3. Result and Discussion

3.1 Optical band gap determination

The band gap is defined as the energy difference between the top of the valence band and the bottom of the conduction band. Electrons are generally able to jump from one band to another as long as a specific minimum amount of energy for the transition, i.e. the band gap energy, is pro- vided. The optical band gap was calculated using absorption edge values (λ edge, in nm) from absorption spectra.

In Fig. (1a) the absorption spectra of pure Sr_2SiO_4 and $Sr_2SiO_4:Eu^{2+}$ (0.1), Dy^{3+} (0.2) are shown in the wavelength range of 200 nm to 500 nm. It can be seen that there is no absorption up to 250 nm and it increases at lower wavelength. The absorption edges found for pure Sr_2SiO_4 and $Sr_2SiO_4:Eu^{2+}$, Dy^{3+} are 225 nm and 230 nm, respectively.

The band gap energy can be determined using the Tauc relation [11-14]. It is a convenient way of studying the optical absorption spectrum of a material. Tauc equation (1) relates the absorption coefficient α and incident photon energy hν by the following relation:

$$\alpha(h\upsilon) = \frac{B(h\nu - E)n}{h\nu} \quad (1)$$

where Eg is the band gap, constant B is the correction coefficient, hν is energy of photon, n is an index which assumes the values 1/2, 3/2, 2 and 3, depending on the nature of electronic transition responsible for the reflection. The value of the exponent n denotes the nature of the sample transition [11].

When n = 2, the equation (1) stands for the direct band gap and the band gap energy can be calculated by the equation:

$$Eg = \frac{hc}{\lambda} \quad (2)$$

Where h is Planck constant, c is speed of light and λ is the related wavelength.

Fig. (1b) shows a plot of (αhν) 2 versus (hν) according to the equation (1) and equation (2), where ν is the light frequency. The plot can be extrapolated by a straight line, giving the direct band gap value at the intercept with energy axis. The estimated values of optical direct band gap in the material are 5.52 eV and 5.4 eV for Sr_2SiO_4 and $Sr_2SiO_4:Eu^{2+}$, Dy^{3+}, respectively. The band gap of pure Sr_2SiO_4 material is of 0.12 eV wider compared to $Sr_2SiO_4:Eu^{2+}$, Dy^{3+}, this confirm that the carrier concentration in a doped material is increased compared to pure Sr_2SiO_4. The new electronic states created below the conduction band of the material may reduce the band gap of the $Sr_2SiO_4:Eu^{2+}$, Dy^{3+}, It was also explained by Vijayalakshmi *et al*. [15], who reported that in Zn doped SnO_2 the band gap value decreased. The optical band gap of $Sr_2SiO_4:Eu^{2+}$, Dy^{3+}, shifts towards the higher wavelength region (visible region) [16].

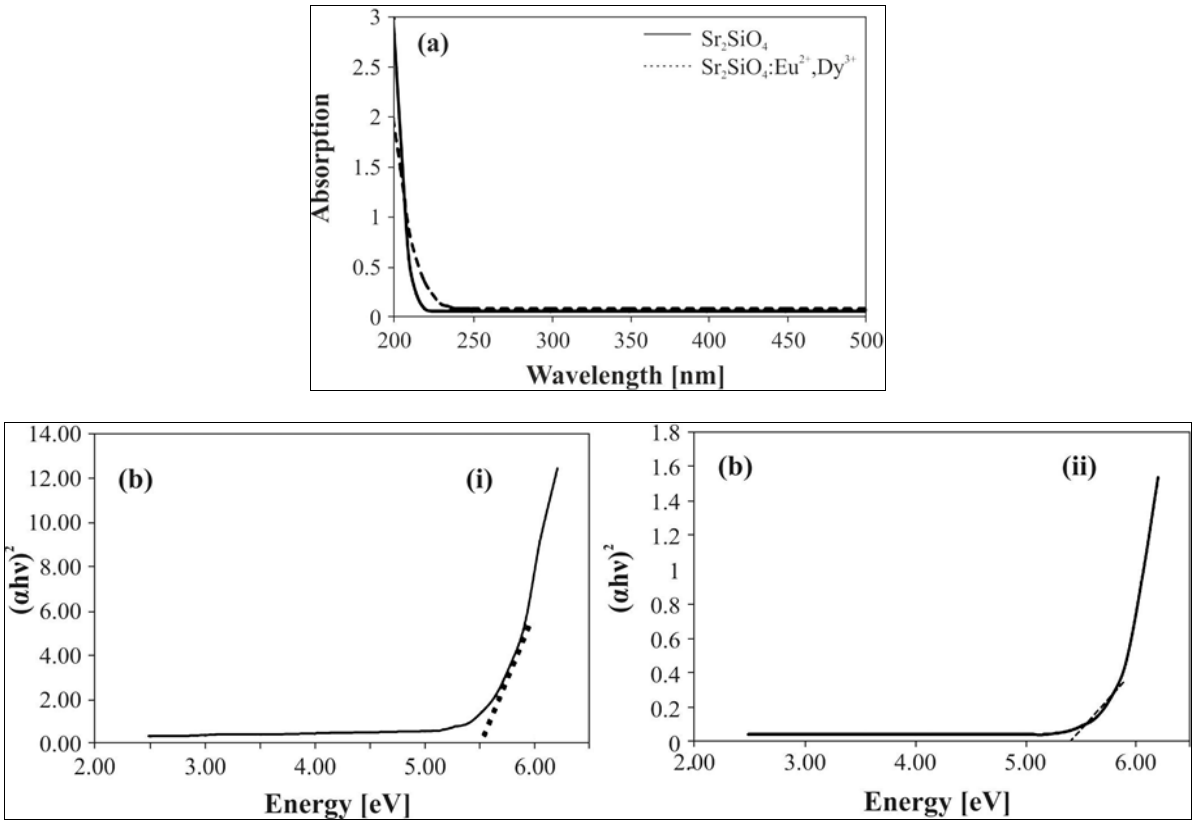

Fig 1: (a) absorption spectra of pure Sr_2SiO_4 and $Sr_2SiO_4:Eu^{2+}$, Dy^{3+} having absorption edges at 225 nm and 230 nm, (b) and (c) plots of (αhν)2 against energy E (eV) with band gap values for (i) Sr_2SiO_4 = 5.52 eV and (ii) $Sr_2SiO_4:Eu^{2+}$, Dy^{3+} = 5.4 eV.

3.2 Structural analysis X-ray diffraction (XRD)

The analysis of XRD data of Sr_2 SiO_4 phase is usually qualitative, just based on relative peak intensities. The typical X-ray diffraction patterns for combustion synthesized Sr_2SiO_4: Eu^{2+} phosphor powders in presence of different Dy^{3+} concentrations are shown in Fig. (2). It can be seen that the diffraction peaks of all the samples could be indexed to the monoclinic phase of β-Sr_2SiO_4 (Ref. code 98-003-5667). An estimation of average crystallite size for the sample is done using Scherer formula [17, 18]

$$L = \frac{0.94\lambda}{\beta \cos\theta} \quad (3)$$

Where L is the crystallite size, λ is the wavelength (for Cu Kα, λ = 1.5406 Å), β is the full width at half maximum (FWHM) and θ is the Bragg's angle. Table 1 shows the calculation results of XRD data for Sr_2SiO_4:Eu^{2+}, Dy^{3+} phosphor. The peaks in XRD patterns of different samples are similar to each other and are attributed to Sr_2SiO_4 monoclinic phase. The calculated average crystallite size of Sr_2SiO_4:Eu^{2+}, Dy^{3+} phosphor is 12.77 nm.

Table 1: XRD data of Sr_2SiO_4:Eu^{2+}, Dy^{3+} doped material.

2θ	I/I₀[%]	FWHM[β]	Crystallite size [nm]	Lattice spacing [Å]	(h k l)
25.0260	20.37	0.7488	10.80	3.55531	(1 1 1)
27.4103	12.49	0.7488	10.91	3.25123	(1 1 3)
30.8088	34.68	0.7488	11.0	2.89989	(0 1 3)
31.3317	100	0.624	13.22	2.85268	(1 0 2)
31.6852	31.51	0.748	11.02	2.82166	(2 0 2)
31.9169	79.86	0.4056	20.36	2.80170	(1 1 3)
39.3022	16.64	0.6240	13.5	2.29057	(2 1 4)
44.0596	22.12	0.7488	11.4	2.05364	(2 2 0)

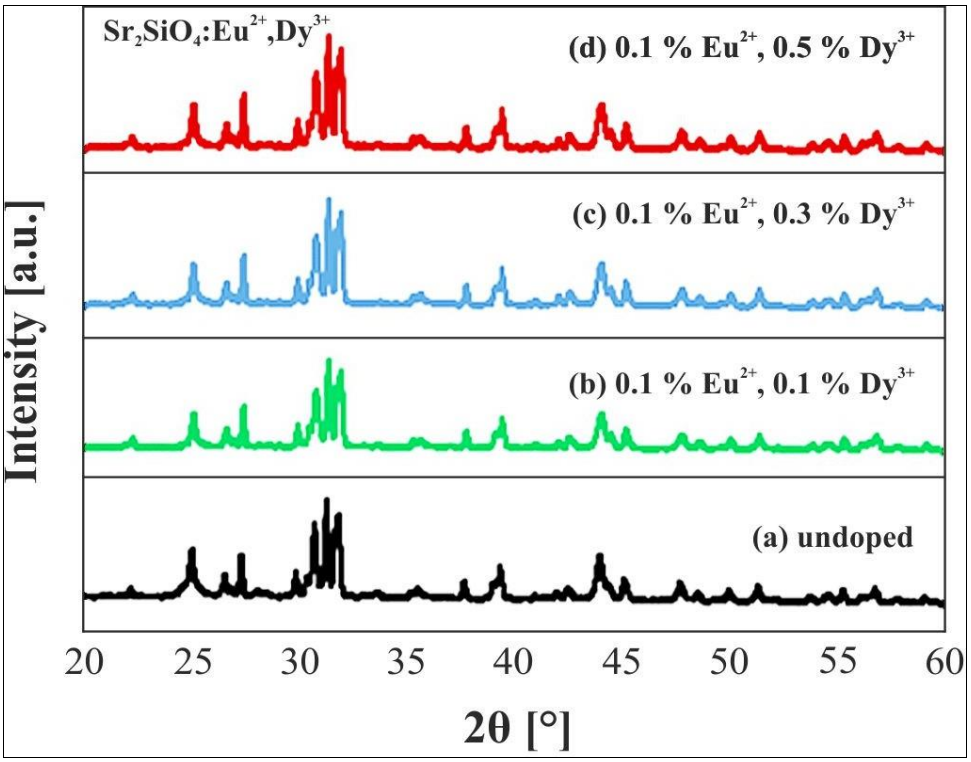

Fig 2: XRD patterns of Sr_2SiO_4:Eu^{2+} phosphors with different Dy^{3+} molar concentration.

3.3 Morphological characterization: Scanning Electron Microscopy (SEM)

The luminescence properties of phosphor particles depend on the morphology of the particles, such as size, shape, defects and so on. The morphology and topography of the samples were studied using scanning electron microscopy (SEM). The surface morphology of the Sr_2SiO_4:Eu^{2+}, Dy^{3+} phosphor is shown in Fig. (3a) and Fig. (3b) at different magnifications. The surface morphology of the particles is not uniform and they form aggregates. The agglomerated particles, pores and voids are the result of gases released during the combustion process [19].

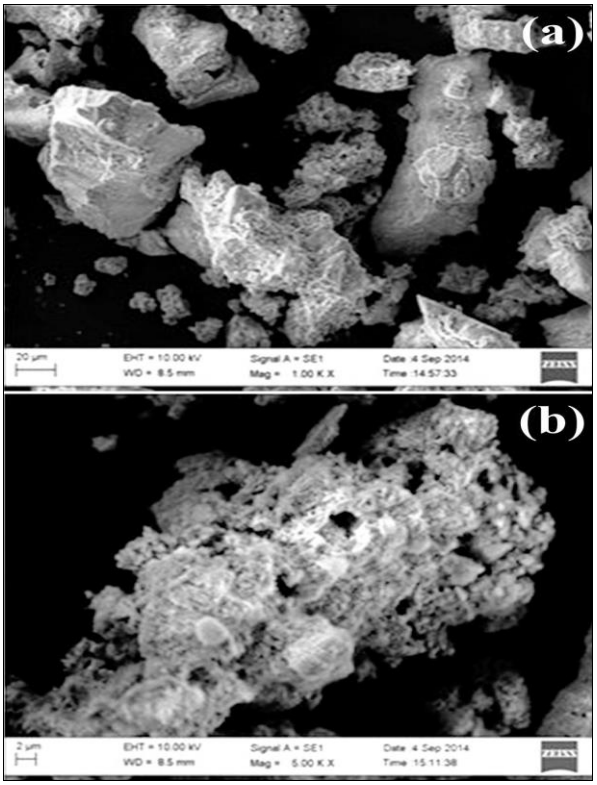

Fig 3: SEM micrographs of $Sr_2SiO_4:Eu^{2+}$, Dy^{3+} phosphor at different magnifications.

3.4 Photoluminescence Studies

The photoluminescence spectra of $Sr_2SiO_4:Eu^{2+}$ (0.1), Dy^{3+} (0.2) are shown in Fig. (4a) and Fig. (4b). The maximum PL intensity was found for Eu^{2+} (0.1) and Dy^{3+} (0.2) doping concentration so we chose this doping concentration for PL measurement. Fig. (4a) shows the excitation spectrum, in the spectral region from 200 nm to 400 nm. It exhibits only one broad peak in the UV region centered at 245 nm. After UV excitation, the phosphor emits visible lights at a wavelength of 485 nm (blue), where a small peak is observed and at 560 nm (yellow) where a broad peak is seen (Fig. 4b). The broad absorption and emission spectra can be ascribed to the Eu^{2+} transition from $4f^7$ state to $4f^75d$ excited state. Here, the luminescence centers correspond to Eu^{2+} ions, and any additional emission peak relating to Dy^{3+} ions in $Sr_2SiO_4:Eu^{2+}$, Dy^{3+} phosphor is not observed. As expected, Dy^{3+} co-doped phosphor show significant long-lasting afterglow properties [20].

Table 2. Calculated kinetic parameters of PL glow curves plotted after different decay times.

Decay time [min]						g	= δ/ω	depth) [eV]
Immediately	308.5	336.07	362.15	27.57	26.43	54	0.49	0.52
5	315.93	344.95	374.3	29.02	29.35	58.37	0.50	0.53
10	315.93	342.47	376.75	27.54	34.28	61.82	0.55	0.58
15	331.6	359.72	388.14	28.12	28.42	56.54	0.50	0.60
20	337	369.42	401	32.42	31.58	64	0.49	0.53
25	338.5	371.86	421	33.36	49.14	82.5	0.59	0.56
30	331.7	374.3	416.3	42.6	42	84.6	0.49	0.41

The decay curve of Sr_2SiO_4: 0.1 mol % Eu^{2+}, 0.2 mol% Dy^{3+} phosphor shown in Fig. (4) At the excitation wavelength of 245 nm generates emission of the wavelength of 560 nm for 120 s. A rapid intensity decrease at the initial stage is ob- served, then it slows down and finally a stable emission is achieved, followed by a slow decay process of long-lasting phosphorescence. $Sr_2SiO_4:Eu^{2+}$, Dy^{3+} phosphors show the persistent luminescence because Dy^{3+} ions play an important role in the afterglow process. The Dy^{3+} ions act as deep whole trap levels, which are located between the ground and excited states of Eu2+. After excitation by UV light, ground states of Eu2+ excitation occurs as a result of electron and whole pair's generation from the ground state 4f to excited 4f 5d state. Some free holes transported into the conduction band are cap- tured by the Dy^{3+} traps. According to Jia *et al.* [21] Dy^{3+} transfers the electron to the excited Eu^{2+}; the states as Dy^{4+} and Eu^{2+} are converted into Eu^{2+}. When UV excitation ends, the reversed route and the recombination of the hole and electron occurs to give bright and long-lasting phosphor [22].

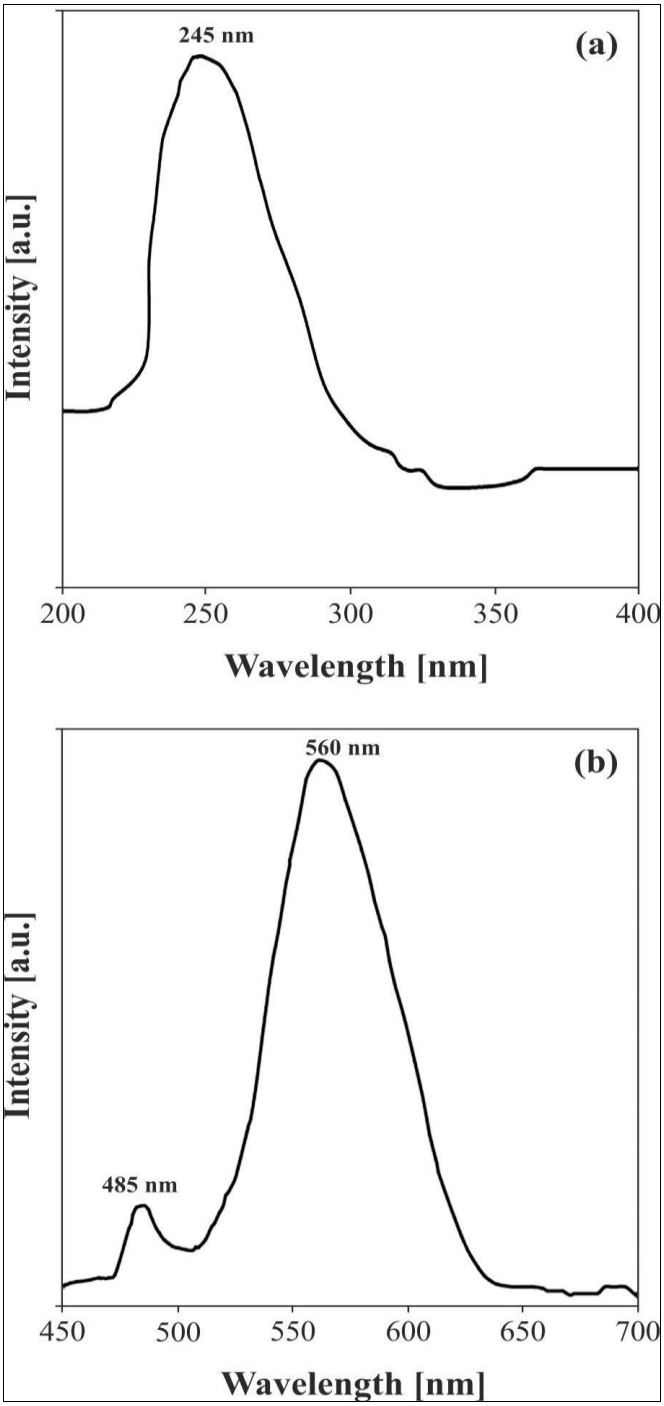

Fig 4: (a) Excitation spectra and (b) emission spectra of $Sr_2SiO_4:Eu^{2+}$ (0.1), Dy^{3+} (0.2) phosphor

4. Conclusion

In this work, $Sr_2SiO_4:Eu^{2+}$, Dy^{3+} phosphor was prepared by combustion method which appears to be a very feasible method for production of this material. The band gaps of 5.52 eV and 5.4 eV for Sr_2SiO_4 and $Sr_2SiO_4:Eu^{2+}$, Dy^{3+}, respectively have been determined from the absorption spectra. Narrowing the band gap of 0.12 eV for $Sr_2SiO_4:Eu^{2+}$, Dy^{3+} compared to pure Sr_2SiO_4 material shows the presence of impurity ions in the host material. XRD studies con- firmed the formation of a single phase compound and the average crystallite size of $Sr_2SiO_4:Eu^{2+}$, Dy^{3+} phosphor was found as 12.77 nm. SEM studies have shown that the particles are non-uniformly distributed in the material and form aggregates. PL spectra of Sr_2 SiO_4 Eu^{2+} (0.1), Dy^{3+} (0.2) phosphor exhibited strong emission peak 560 nm (yellow) and a weak 485 nm (blue) emission, when the phosphor was excited by 245 nm under UV region. The PL exponential decay curve showed that the phosphor has good luminescence properties.

5. References

1. Ayvacıklı M, Ege A, Yercı S, Can N. J Lumin. 2011;131:24SA32
2. Matsuzawa T, Aoki Y, Takeuchi N, Murayama Y. J Electrochem Soc. 1996;143:2670.
3. Catti M, Gazzoni G, Ivaldi G, Zanini G. Acta Crystallogr C. 1983;39:29.
4. Hyde BG, Sellar JR, Stenberg L. Acta Crystallogr B. 1986;42:423.
5. Stenberg L, Hyde BG. Acta Crystallogr B. 1986;42:417.

6. Wu ZC, Shi JX, Gong ML, Wang J, Su Q. Mater Chem Phys. 2007;103:415.
7. Briche S, Zambon D, Boyer D, Chadevron G, Mahiouet R. Opt Mater. 2006;28:615.
8. Wu C, Wang Y, Jie W. J Alloy Compd. 2007;436:383.
9. Chakradhar RPS, Nagabhushana BM, Chandrappa GT, Ramesh KP, Rao JL. J Chem Phys. 2004;121:10250.
10. Haranath D, Chander H, Sharma P, Singh S. Appl Phys Lett. 2006;89:173118.
11. Tauc J, Menth A. J Non-Cryst Solids. 1972;8-10:569.
12. Tauc J. Mater Res Bull. 1968;3:37.
13. Tauc J, Grigorovici R, Vancu A. Phys Status Solidi B. 1966;15:627.
14. Buchholz DB, Liu J, Marks TJ, Zhang M, Chang RPH. ACS Appl Mater Inter. 2009;1:2147.
15. Vijayalakshmi S, Venkataraj S, Subramanian M, Jayavel R. J Phys D. 2008;41:035505.
16. Mayandi J, Marikkannan M, Ragavendran V, Jayabal P. J Nanosci Nanotechnol. 2024;2:707.
17. Feitosa AV, Miranda MAR, Sasaki JM, Araujo-Silva MA. Braz J Phys. 2004;34:656.
18. Ubale AU, Sangawar VS, Kulkarni DK. B Mater Sci. 2007;30:147.
19. Sunitha DV, Manjunatha C, Shilpa CJ, Nagabhushana H, Sharma SC, Nagabhushana BM. Spectrochim Acta A. 2024;99:279.
20. Matsuzawa T, Aoki Y, Takeuchi N, Murayama Y. J Electrochem Soc. 1996;143:2670.
21. Jia W, Yuan H, Lu L, Liu H, Yen WM. J Lumin. 1998;76:424.
22. Yamamoto H, Matsuzawa T. J Lumin. 1997;72:287.